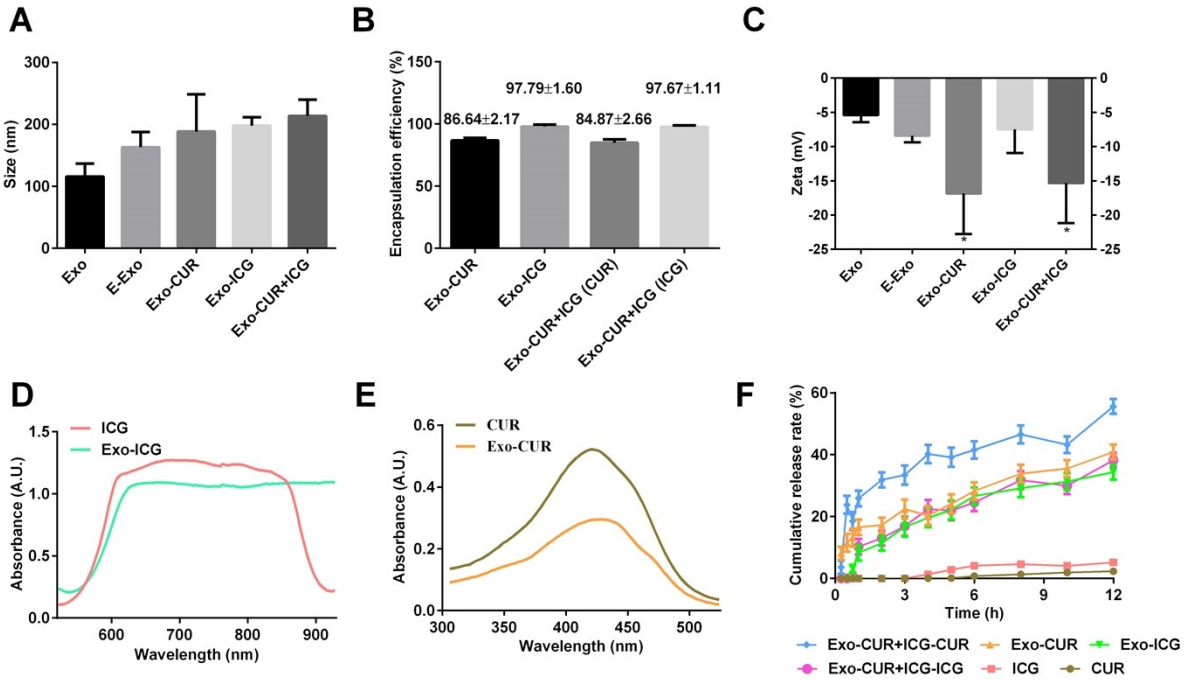

Figure S1. Physicochemical characterizations of the engineered Exo. (A) Particle sizes. (B) Encapsulation efficiencies calculated by Eq. 1. (C) Zeta potentials. (D, E) UV-vis detection of CUR and ICG before and after encapsulation into Exo. (F) *In vitro* drug release profiles of engineered Exo for 12 h. Exo-CUR+ICG-CUR: encapsulation of CUR in the Exo-CUR+ICG group; Exo-CUR+ICG-ICG: encapsulation of ICG in the Exo-CUR+ICG group. Each bar represents the mean±SD of three replicates. $^{**}p < 0.01$, $^{*}p < 0.05$.

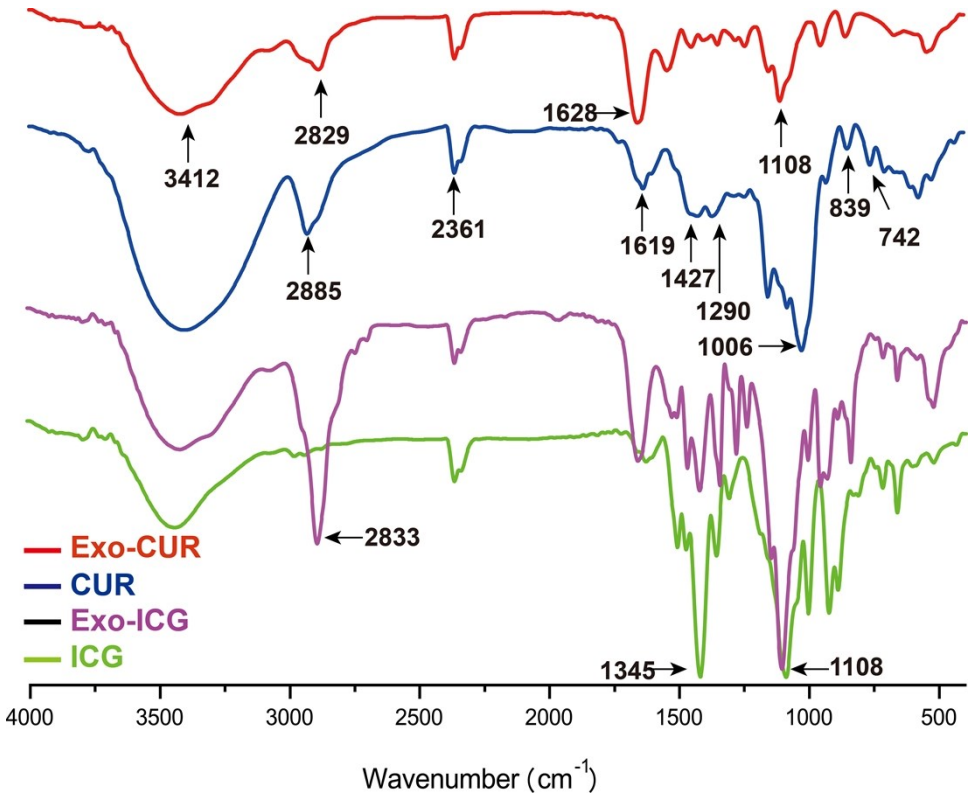

Figure S2. FTIR spectra of Exo-CUR, CUR, Exo-ICG and ICG in the wavenumber range of 400-4000 cm^{-1}.

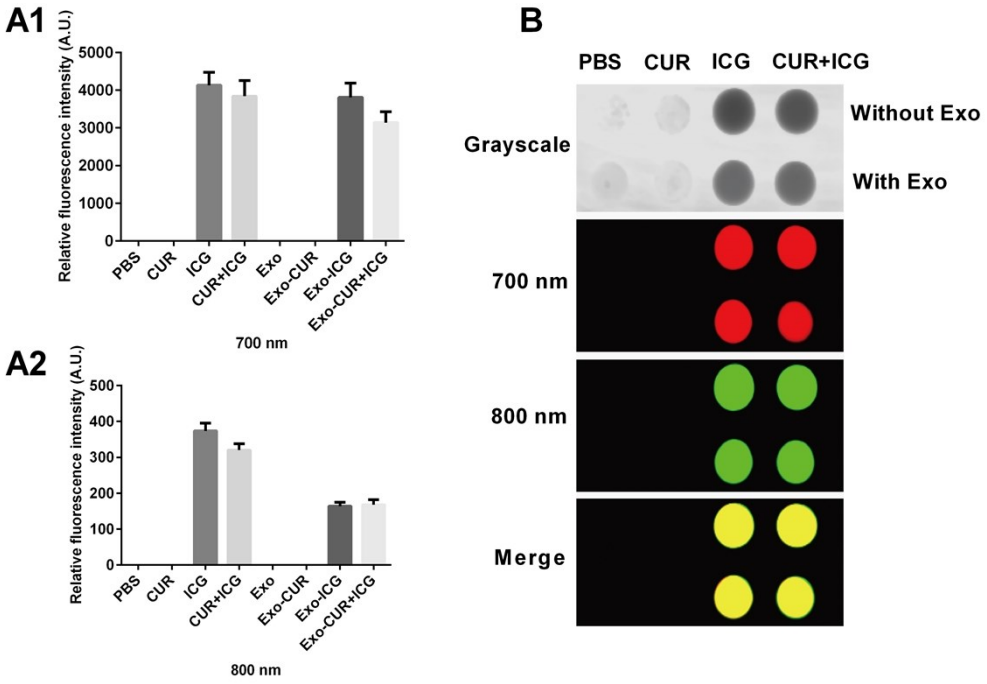

Figure S3. Quantitative fluorescence intensity comparisons of original drugs and Exo-incorporated drugs under NIR irradiation at (A1) 700 nm and (A2) 800 nm, respectively. (B) Qualitative fluorescence images of free drugs and Exo-incorporated drugs under NIR irradiation. Each bar represents the mean±SD of three replicates.

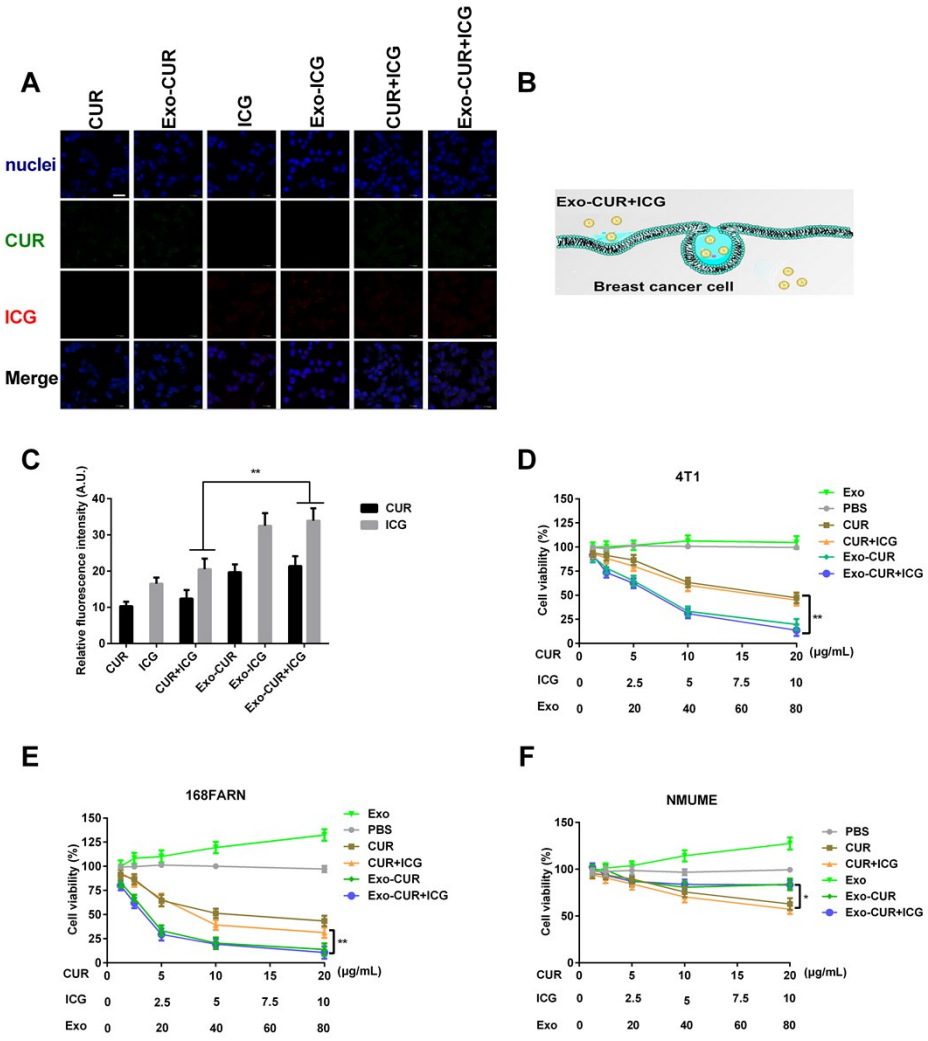

Figure S4. (A) Fluorescence images showing intracellular uptake of engineered Exo into 4T1 cells within 0.5 h of co-incubation; scale bar: 20 μm. (B) Illustration displaying the transportation mechanism of engineered Exo into cancer cells. (C) Quantitative cell uptake efficiencies of CUR, ICG, CUR+ICG, and engineered Exo (containing 10 μg/mL CUR or ICG) within 6 h. (D, E) Anticancer effects against breast cancer cell lines 4T1 and 168FARN, respectively. (F) Cytotoxicity of engineered Exo against normal breast cell line NMUME at different concentrations of encapsulated CUR. Each experiment was performed in triplicates.

Each bar represents the mean±SD of six replicates. Statistical significance is expressed as **p < 0.01, *p < 0.05.

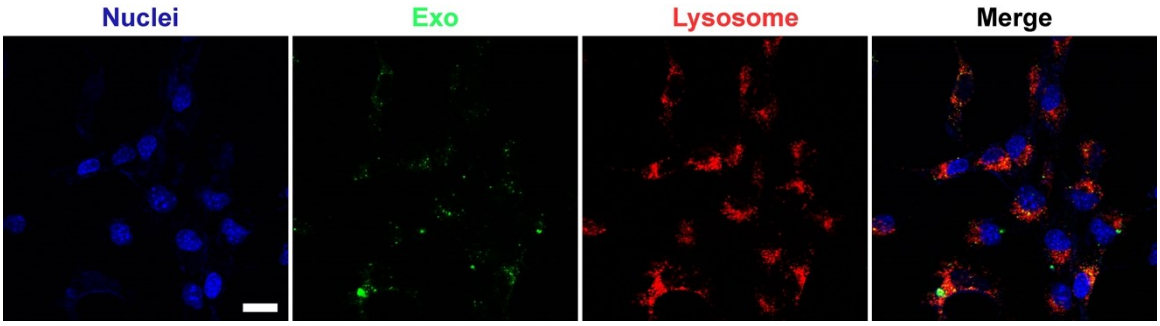

Figure S5. Fluorescence images showing the intracellular fate of Exo (50 μg/ml) within 4T1 cells at 24 h; scale bar: 20 μm.

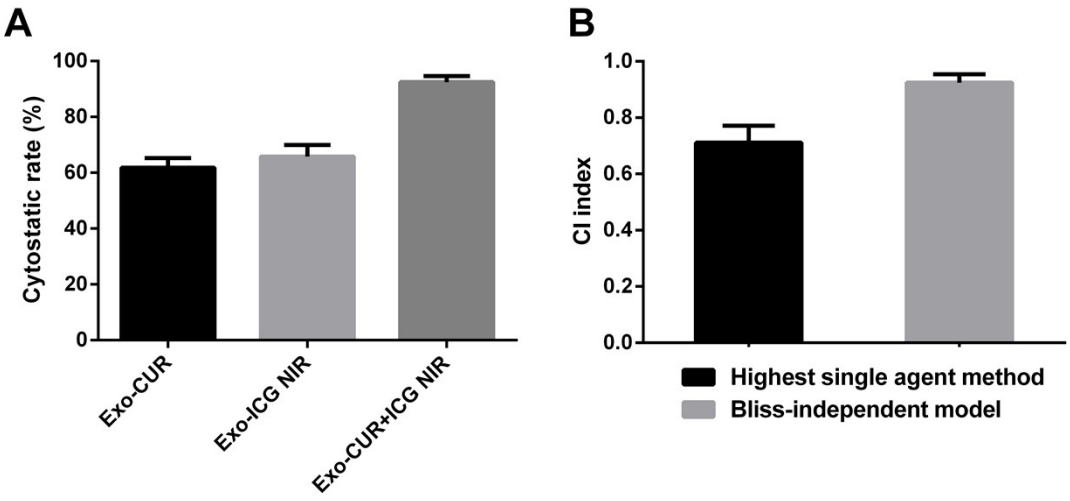

Figure S6. Calculation of cooperativity. (A) Cytostatic rate of 4T1 cells treated with Exo-CUR, Exo-ICG, and Exo-CUR+ICG under NIR irradiation. (B) The CIs were calculated by the "Highest single agent (HSA)" and the "Bliss Independence". Each bar represents the mean±SD of three replicates.

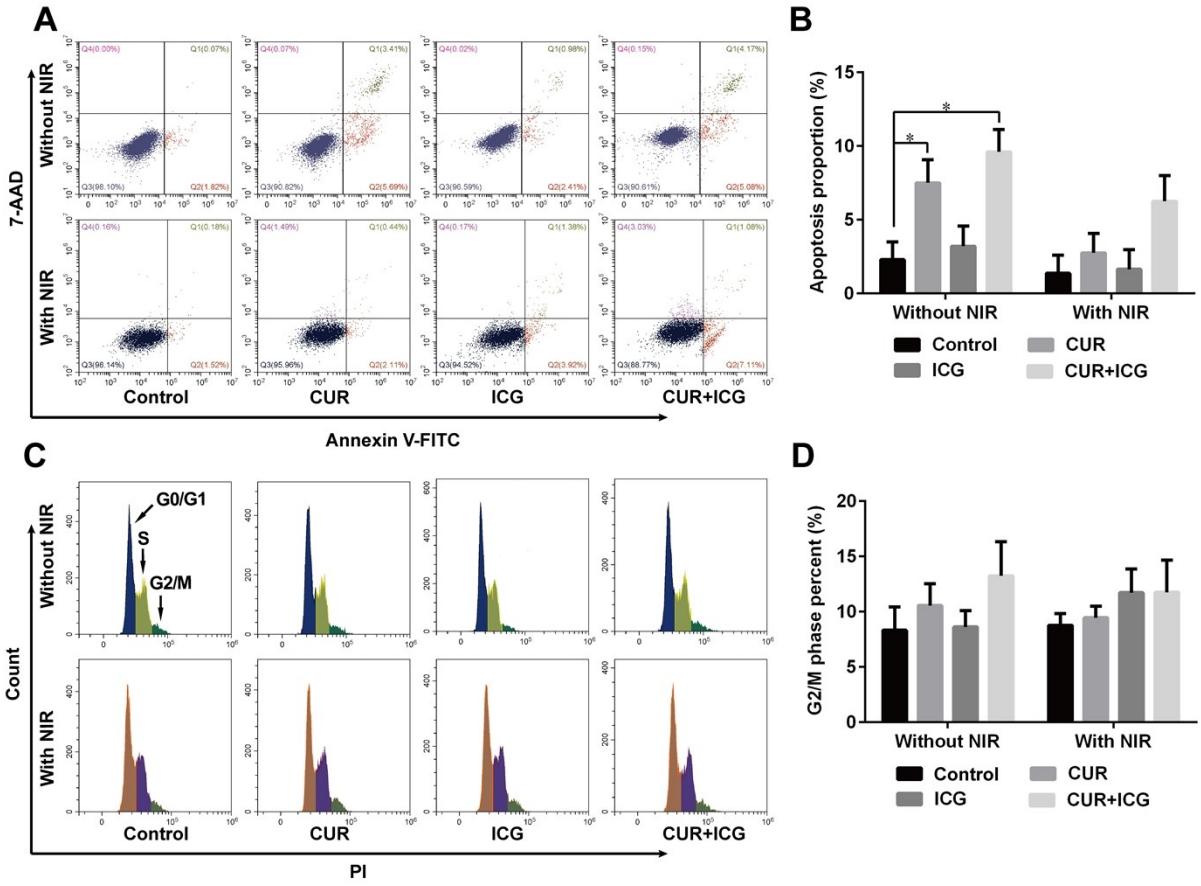

Figure S7. (A) Qualitative apoptotic progression and (C) cell cycle of 4T1 cells in response to samples with and without NIR irradiation. (B) Quantitative analyses of FACS distributions (%) and (D) G2/M phase of 4T1 cells in response to different groups with and without NIR irradiation. Total apoptosis includes late apoptosis plus early apoptosis. Each bar represents the mean±SD of six replicates. Statistical significance is expressed as *$p < 0.05$.

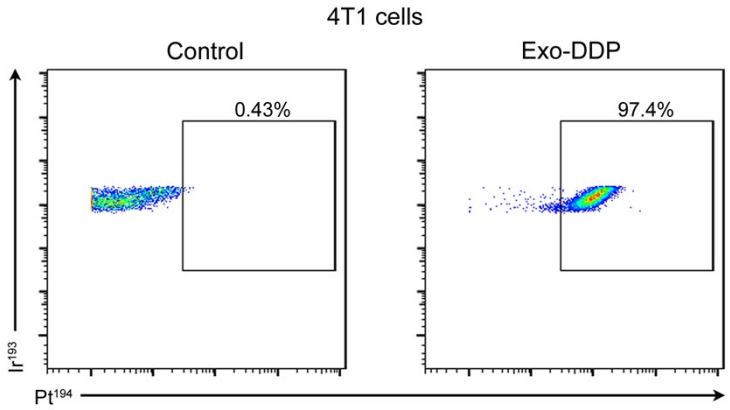

Figure S8. 4T1 cells were incubated with Exo-DDP for 24 h and the Pt^{194} signals in these cells were successfully detected using mass cytometry.

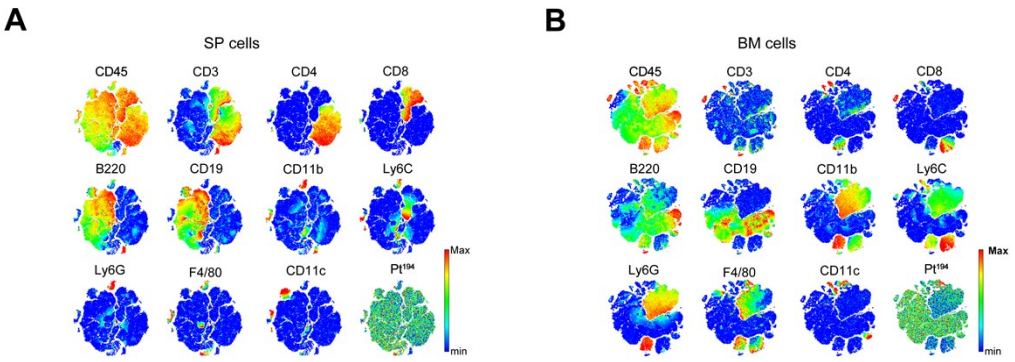

Figure S9. (A, B) Expressions of 11 markers and Pt194 signals on the viSNE maps of (A) spleen or (B) BM cells.

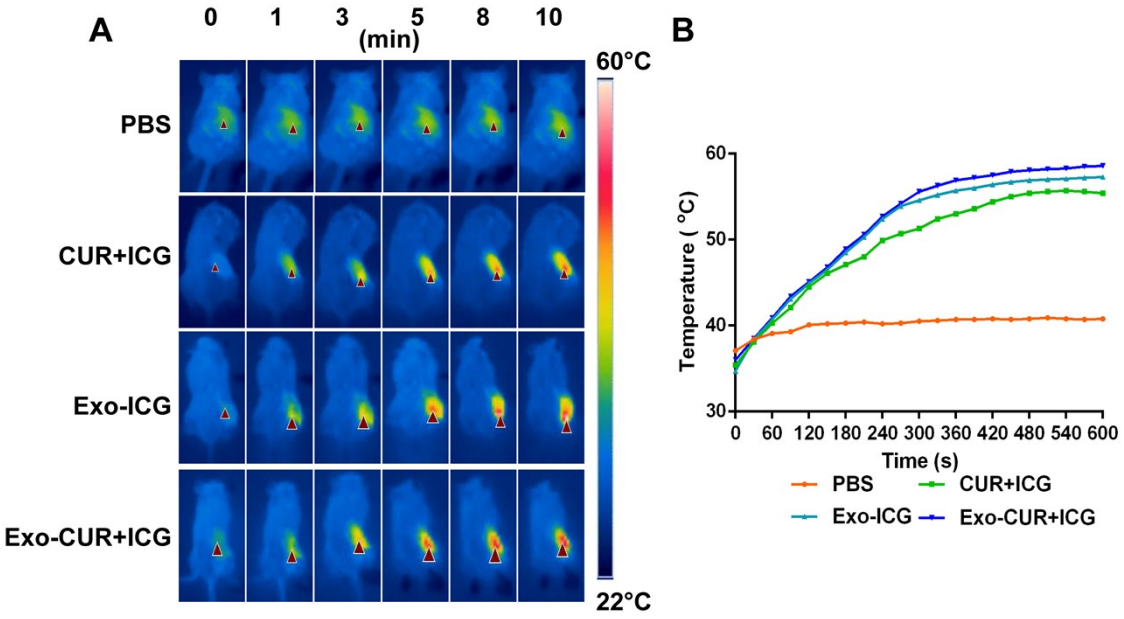

Figure S10. *In vivo* PTT of engineered Exo. (A) Thermal images showing NIR-induced (2 W/cm^2 for 10 min) photothermal therapeutic effects within tumors at different time points. (B) Temperature changes of engineered Exo within tumors after NIR irradiation.

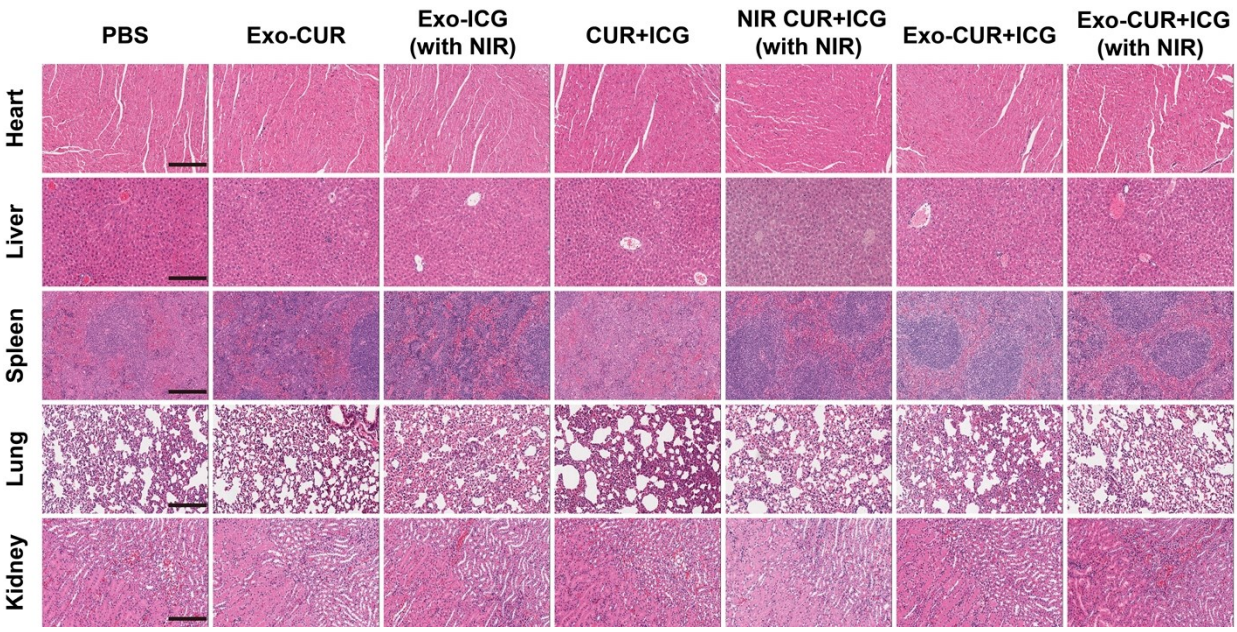

Figure S11. H&E-stained histopathological images showing major organs in breast tumor-bearing mice treated by different samples with and without NIR irradiation; scale bars: 200 μm.